PSFC/JA-08-27

Observations of Counter-Current Toroidal Rotation in Alcator C-Mod LHCD Plasmas

J. E. Rice, A.C. Ince-Cushman, P. T. Bonoli, M. J. Greenwald , J.W. Hughes, R.R. Parker, M.L. Reinke, G.M. Wallace, C.L. Fiore, R.S. Granetz, A.E. Hubbard, J.H. Irby, E.S. Marmar, S. Shiraiwa, S.M. Wolfe and S.J. Wukitch, M. Bitter*, K. Hill* and J.R. Wilson*

October 2008

Plasma Science and Fusion Center
Massachusetts Institute of Technology
Cambridge MA 02139 USA

** Princeton Plasma Physics Laboratory, Princeton, NJ*

This work was supported by the U.S. Department of Energy, Grant No. DE-FC02-99ER54512.

Submitted for publication to *Physical Review Letters.*

Observations of Counter-Current Toroidal Rotation in Alcator C-Mod LHCD Plasmas

J.E. Rice, A.C. Ince-Cushman, P.T. Bonoli, M.J. Greenwald,
J.W. Hughes, R.R. Parker, M.L. Reinke, G.M. Wallace, C.L. Fiore, R.S. Granetz,
A.E. Hubbard, J.H. Irby, E.S. Marmar, S. Shiraiwa, S.M. Wolfe and S.J. Wukitch
Plasma Science and Fusion Center, MIT, Cambridge, MA 02139-4307

M. Bitter, K. Hill and J.R. Wilson
Princeton Plasma Physics Laboratory, Princeton, NJ

Abstract

Following application of lower hybrid current drive (LHCD) power, the core toroidal rotation in Alcator C-Mod L- and H-mode plasmas is found to increment in the counter-current direction, in conjunction with a decrease in the plasma internal inductance, l_i. Along with the drops in l_i and the core rotation velocity, there is peaking of the electron and impurity density profiles, as well as the ion and electron temperature profiles. The mechanism generating the counter-current rotation is unknown, but it is consistent with an inward shift of energetic electron orbits, giving rise to a negative core radial electric field. The peaking in the density, toroidal rotation (in the counter-current direction) and temperature profiles occurs over a time scale similar to the current relaxation time but slow compared to the energy and momentum confinement times. Most of these discharges exhibit sawtooth oscillations throughout, with the inversion radius shifting inward during the LHCD and profile evolution. The magnitudes of the changes in the internal inductance and the central rotation velocity are strongly correlated and found to increase with increasing LHCD power and decreasing electron density. The maximum effect is found with a waveguide phasing of 60° (a launched parallel index of refraction $n_{\|}\sim 1.5$), with a significantly smaller magnitude at 120° ($n_{\|}\sim 3.1$), and with no effect for negative or heating (180°) phasing. These results resemble the current drive efficiency which scales as $P_{LH}/n_e {n_{\|}}^2$. Regardless of the plasma parameters and launched $n_{\|}$ of the waves, there is a strong correlation between the rotation velocity and l_i changes, possibly providing a clue for the underlying mechanism.

I. Introduction

In order for tokamaks to be viable candidates for future steady state fusion reactors, some variety of non-inductive current drive is necessary. Lower hybrid current drive (LHCD) [1] has been successfully implemented in lower electron density plasmas [2, 3, 4], and an outstanding issue is the extension to higher densities and under conditions relevant for reactors [5]. Another approach for non-inductive current drive is to take advantage of the bootstrap current [6] generated by the large pressure (density and temperature) gradients in plasmas with internal transport barriers (ITBs) [7, 8]. Challenges of this approach involve production of steady state ITBs (without current ramping) under reactor relevant conditions (without neutral beam injection) and control of the barrier foot location. H-mode plasmas with ITBs having pressure gradients in excess of 2.5 MPa/m have been obtained in Alcator C-Mod with ion cyclotron range of frequencies (ICRF) heating [9, 10, 11, 12, 13, 14]. ITBs have also been formed without neutral beam injection in lower hybrid current drive (LHCD) and electron cyclotron current drive (ECCD) plasmas in other devices [15, 16, 17]. Another issue for future tokamak reactors is the generation and control of rotation velocity profiles for resistive wall mode (RWM) suppression [18, 19] in the absence of external momentum input [20].

The areas of LHCD [5], ITB formation [14] without current ramping or external momentum input and self-generated flows [21] are important components of the Alcator C-Mod research program, and will all be addressed here. C-Mod [22] is a compact (R$\sim$0.67 m, r$\sim$0.21 m), high field ($B_T \leq 8$ T) device which can operate with electron densities in the range of 10^{19}-10^{21}/m^3. Auxiliary heating is provided with up to 6MW of ICRF power. Dimensionless plasma parameters in the following ranges have been achieved: $0.2 \leq \beta_N \leq 1.8$, $0.01 \leq \nu^* \leq 20$ and $170 \leq 1/\rho^* \leq 500$. Non-inductive current is driven with LH waves injected from an 88 waveguide launcher capable of delivering up to 1.2 MW of power at 4.6 GHz with a parallel index of refraction, $n_{\|}$, in the range of 1.5-4 (waveguide phasing between 60° and 150°), in both the co- and counter-current direction [5]. Time resolved toroidal rotation velocity and ion temperature profiles have been measured with an imaging Johann x-ray spectrometer system, from the Doppler shifts and broadening of argon and molybdenum x-ray emission lines [23]. Central chord rotation velocities also come from a tangentially viewing von Hamos type x-ray spectrometer. Electron density profile evolution was determined using a laser interferometer and Thomson scattering system, electron temperature profiles were measured using Thomson scattering and a variety of ECE diagnostics and x-ray emission profiles were recorded with a diode array [24]. Current density profile measurements were not available for the discharges presented here; information on the current density comes from the internal inductance (l_i, a measure of the peakedness of the current density profile), observations of sawtooth patterns and EFIT [25] magnetics reconstructions.

An outline of the paper is as follows: LHCD discharge time histories and parameter profiles will be presented in II, followed by scaling studies in III, with a discussion and conclusions in IV.

II. Observed Rotation Time Histories and Profile Evolution

In order to optimize performance in advanced tokamak operation, LHCD has been applied to a variety of different plasma types under a wide parameter range: lower, double and upper null L-mode target discharges with B_T in the range from 3.8 to 6.2 T, currents from 0.6 to 1.0 MA and electron densities from 0.4 to 1.2 $\times$ 10^{20}/m^3, in addition to H-mode target plasmas. LHCD power levels between 0.4 and 1.1 MW have been injected with $n_{\|}$ in the range of 1.5-4, both co- and counter-current, including pure heating phasing. Shown in Fig.1 are the time histories of several parameters of interest for a low density 5.4 T, 0.8 MA L-mode discharge with LHCD. Following application of 0.8 MW of power between 0.8 and 1.3 s (with a launched $n_{\|} \sim$ 2.3), there was an increase in the core electron density and temperature, a drop in the

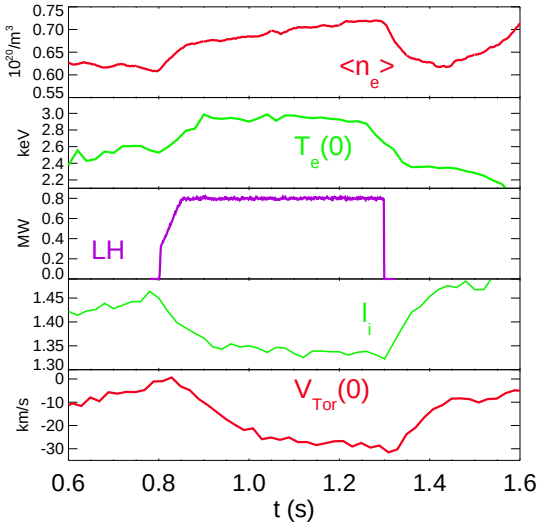

Figure 1: The average electron density, electron temperature, LHCD power, internal inductance and central toroidal rotation for a 5.4 T, 0.8 MA L-mode discharge.

internal inductance (consistent with a broadening of the current density profile) and an increment of the central toroidal rotation velocity in the counter-current direction [26]. (Here a negative velocity corresponds to counter-current rotation.) Modeling indicates that about 250 kA were driven by LH waves in this case. The time scale for the change in the velocity is on the order of hundreds of ms, similar to the current relaxation time ($\tau_{\rm CR}$=1.4a$^2\kappa$T$_e{}^{1.5}$/Z$_{eff}$ $\sim$ 250 ms), but much longer than the energy [27] or momentum [28, 29] confinement times ($\sim$35 ms). The time evolutions of the internal inductance and the toroidal rotation velocity are similar, suggesting a connection between the two quantities. Shown in Fig.2 is a comparison of two nearly identical

5.4 T, 0.8 MA L-mode target plasmas, with and without 0.4 MW of LHCD power at a launched $n_{||} \sim 2.3$, which highlights the effect of a peaking of the electron density, a broadening of the current density profile and a change of the rotation velocity in

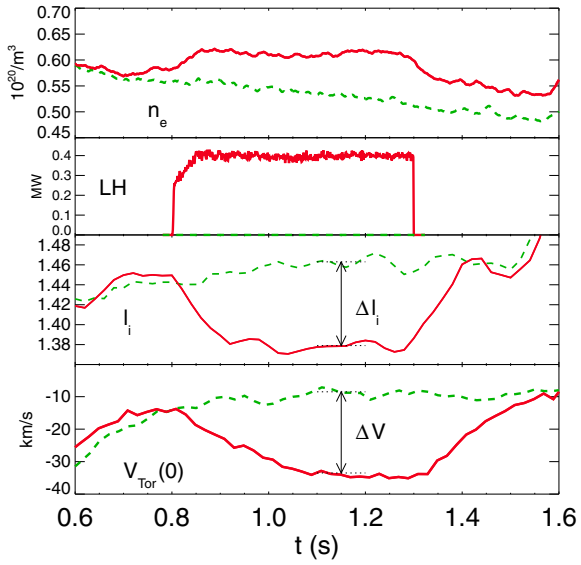

Figure 2: A comparison of two similar discharges, with (red solid) and without (green dashed) LHCD. From top to bottom, the electron density, LHCD power, internal inductance and central toroidal rotation velocity.

the counter current direction. The change in the internal inductance between the two discharges at 1.2 s was $\Delta l_i \sim -0.070$, while the change in the core rotation velocity was ΔV~ -24 km/s. Most C-Mod Ohmic L-mode discharges exhibit counter-current rotation [30, 31]; application of LHCD leads to even stronger counter rotation. The magnitude of the changes in the internal inductance and core rotation velocity depend on the $n_{||}$ spectrum of the launched waves [26]. Shown in Fig.3 is a comparison of two similar plasmas with different waveguide phasings. The discharge shown in red had an $n_{||} \sim 1.55$ and demonstrated a much larger drop in l_i and $V_{\rm Tor}$ than the discharge shown in green dashed, with $n_{||} \sim 2.3$. This further emphasizes the connection between the rotation and internal inductance in LHCD plasmas.

A similar counter-current increment in the rotation velocity with LHCD is observed in H-mode target discharges. Shown in Fig.4 are the time histories for a 5.4 T, 0.6 MA double null plasma, which had 1.6 MW of ICRF power delivered between 0.6 and 1.5 s. The H-mode transition time was 0.69 s, as seen by the increases in the electron density and the co-current rotation velocity [32, 33, 9, 29]. With the additional application of 0.9 MW of LHCD power with $n_{||} \sim 2.3$ between 1.1 and 1.4 s, there was an increment of the central toroidal rotation in the counter current direction, though the net rotation

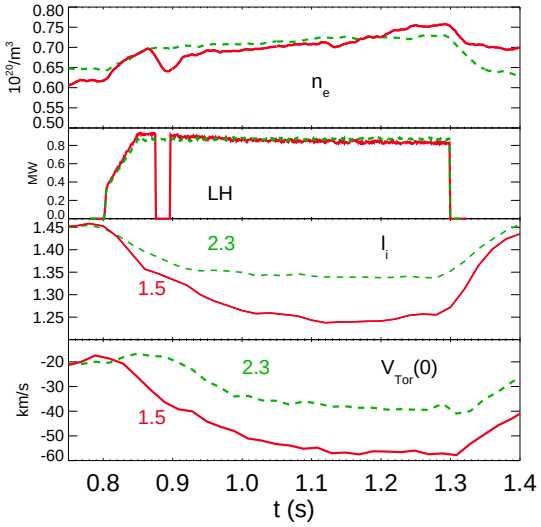

Figure 3: A comparison of two similar discharges with $n_{||} \sim 1.55$ (red solid) and $n_{||} \sim 2.3$ (green dashed). Same legend as in Fig.2.

was still in the co-current direction. Similarly, there was a reduction in the internal inductance. While the average electron density dropped during the LHCD pulse, the profile actually peaked. Although the detailed mechanism giving rise to the changes in rotation is unknown, it cannot be due to changes exclusively in viscous damping, since in L-mode plasmas the magnitude of the rotation increases, while in H-mode it decreases.

Some of the lowest density target discharges develop locked modes, which causes the rotation to stop [29]. Shown in Fig.5 is a plasma with an average electron density of $5.5\times10^{19}/m^3$ at the time of the initiation of LHCD. The internal inductance and core rotation velocity both dropped at first, but as a locked mode developed at 0.93 s, as seen on the magnetics trace, the rotation velocity halted and there was an increase in l_i. Similar behavior has been reported from ASDEX [34]. Mode locking is well known to cause rotation braking [35, 36] but why this affects the current density profile, as seen in the increase of the internal inductance, is not clear. Energy confinement is known to degrade with locked modes and it may be that fast electron confinement also degrades; this loss of fast electrons leads to a reduction of current drive.

The increases in density and temperature, and drops in rotation during LHCD occur in the very core of the plasma [26]. Shown in Fig.6 are the density, velocity and temperature profiles for the discharge of Fig.1 at two different times, before (0.75 s) and during (1.15 s) LHCD. There is a peaking of the electron density profile inside of R = 0.775 m (r/a $\sim$ 0.4) during LHCD, while outside of this radius the profile remains

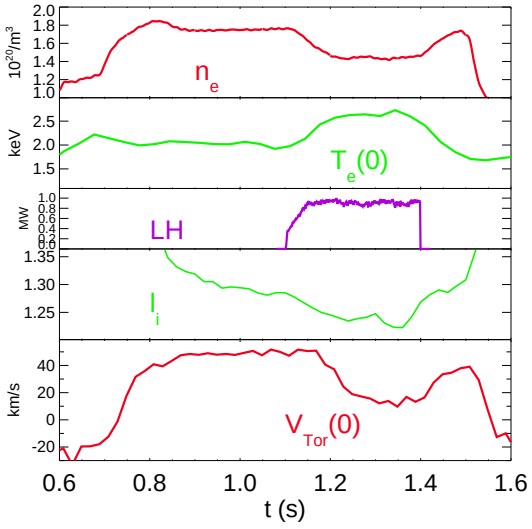

Figure 4: Parameter time histories for an ICRF H-mode discharge with LHCD. Same legend as in Fig.1.

unchanged. Similar behavior is seen in the electron and ion temperature profiles, with a peaking occurring inside of R = 0.755 m during LHCD. Before LHCD, the velocity profile is rather flat and close to stagnant, while during LHCD, the profile is strongly centrally peaked in the counter-current direction. During LHCD, the sawtooth inversion radius moves inward to R $\sim$ 0.73 m from the target location of R $\sim$ 0.76 m. All of the profiles are relatively flat inside of the inversion radii both before and during LHCD. A flattening of the rotation velocity profile inside of the sawtooth inversion radius has been observed in TCV plasmas [37, 38].

A set of profiles for a 0.8 MA, 6.2 T discharge with 0.8 MW of LHCD power at a launched $n_{||} \sim 1.55$ is shown in Fig.7. During LHCD, the central velocity reached 55 km/s in the counter direction, and there were no sawtooth oscillations at this time. Peaking in all profiles was observed inside of R = 0.77 m, indicating a close relationship between the particle, momentum and energy channels.

III. Scalings

Parameter scans of target plasma density, LHCD power and waveguide phasing have been undertaken in order to optimize performance. Shown in Fig.8 are results from a shot to shot power scan with a launched $n_{||} \sim 2.3$ into 0.8 MA, 5.4 T target plasmas. In the top frame is the density peaking factor, the ratio of the central density

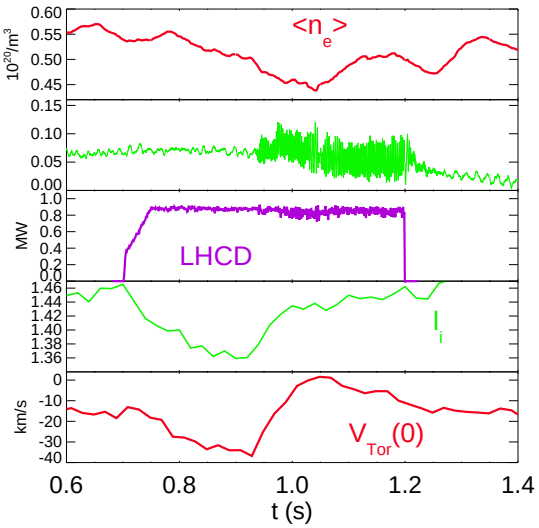

Figure 5: A LHCD plasma with a locked mode, which developed at 0.93 s, as seen in the second panel, which represents the difference between signal levels on two partial flux loops.

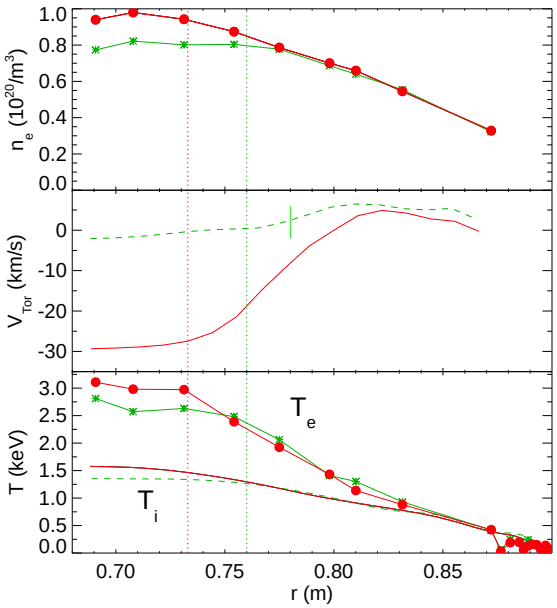

Figure 6: Electron density (top), toroidal rotation velocity (middle) and electron and ion temperature (bottom) profiles before (green dashed, asterisks) and during (solid red, dots) LHCD. Vertical lines indicate the approximate locations of the sawtooth inversion radii.

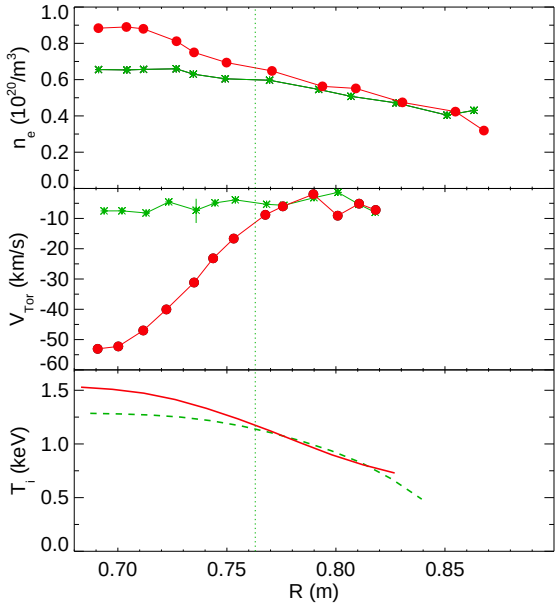

Figure 7: Electron density, rotation velocity and ion temperature profiles, with the same legend as in Fig.6.

to that at r/a = 0.7; there is a steady increase in the density peaking with LHCD power. Similar behavior is seen in the ion temperature, as shown in the middle frame; the change in the central ion temperature (compared to the pre-LHCD level) also increases with injected power. In the bottom frame is the magnitude of the change in the central rotation velocity (always in the counter-current direction), comparing before and during LHCD, and there is a similar scaling with power. The vertical bands of points near the power level of 0.44 MW are due to variations in electron density. Shown in Fig.9 are the same three peaking parameters as a function of electron density for a series of 0.8 MA, 5.4 T discharges at fixed power (0.42 to 0.47 MW) with $n_{||} \sim 2.3$. For all three of these parameters, there is a decrease with increasing electron density. The velocity scalings of Figs.8 and 9 have been combined, including additional 0.8 MA, 5.4 T discharges with $n_{||} \sim 2.3$ LHCD, and are presented in Fig.10, which shows the change in the central rotation velocity as a function of power normalized to the electron density. This figure unifies the trends with LHCD power and electron density, and suggests a similarity to the current drive efficiency, which scales the same way. Similar behavior in the density and temperature profile peaking also holds.

As is evident from Figs.1-5, the changes in internal inductance and rotation velocity are well correlated, regardless of plasma conditions or launched $n_{||}$. This point is emphasized in Fig.11 which shows the magnitude of the change in the rotation velocity as a function of the change in l_i (as defined in Fig.2), for a large number of discharges, regardless of plasma or LHCD parameters. The points in this figure represent a range

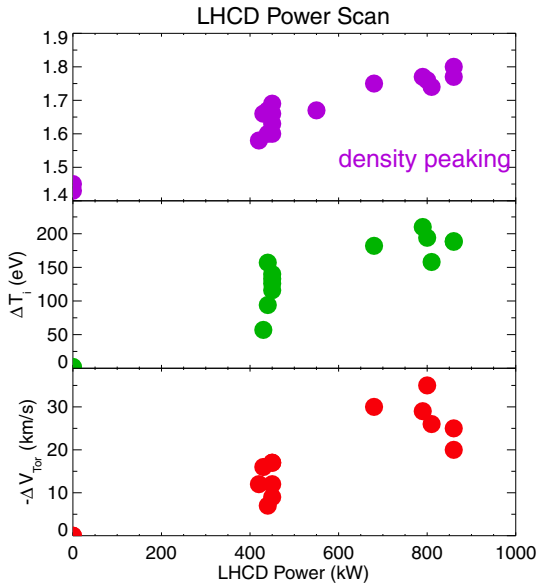

Figure 8: Density peaking factor (top), change in the central ion temperature (middle) and the change in the central rotation velocity (bottom) as a function of LHCD power.

of electron density from 0.4 to 1.2 $\times$ 10 ^{20}/m^3, toroidal magnetic field from 3.8 to 6.2 T, plasma current from 0.6 to 1.0 MA and LHCD power from 0.4 to 1.1 MW, with a variety of magnetic configurations. The points are sorted by launched $n_{||}$ between $\sim$ 1.5 and 3.1. For waves directed counter-current, with $n_{||} \sim -1.5$ and -2.3, there is very little effect.

IV. Discussion and Conclusions

Counter-current rotation during LHCD implies that the radial electric field is negative in the core region [26]. E_r profiles before and during LHCD for the discharge of Figs.1 and 6 are shown in Fig.12. E_r was determined from the radial force balance equation using the measured argon toroidal and poloidal rotation velocity profiles, with the measured argon pressure profiles, and calculated toroidal and poloidal magnetic fields. In this case E_r is dominated by the toroidal rotation velocity term. Before LHCD, the core radial electric field is close to zero, while with LHCD, there is a strong negative E_r which peaks at a value of -13 kV/m near r/a = 0.3. A negative core E_r indicates that there is an inward shift of electron orbits (or an outward shift of ion orbits). The fast electrons generated by LHCD experience an increase in $|v_{||}|$ and hence an increase in their curvature drift velocity, whose sign is such that their orbits contract [26]. These fast electrons slow down through collisions on flux surfaces radially inward of

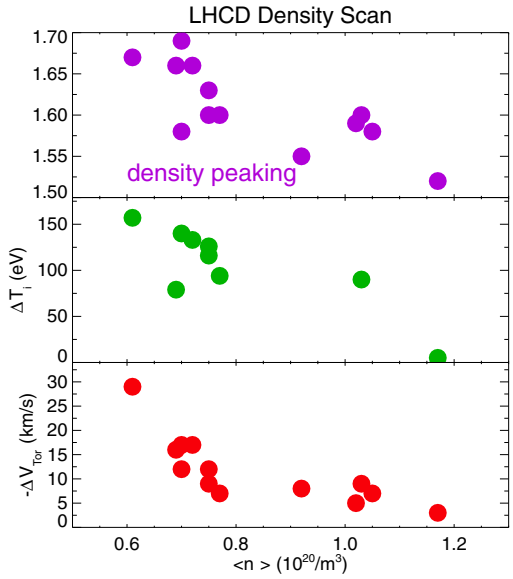

Figure 9: Peaking parameters (as in Fig.8) as a function of electron density at fixed LHCD power.

the ones on which they were born, which constitutes a radial current and results in a negative E_r. Another possible mechanism for the negative core E_r is a resonant trapped particle pinch [39], which results from the canonical angular momentum absorbed by the trapped electrons which interact with the LH waves. Since the resonant particles are relatively collisionless, the added momentum cannot be readily lost, and they are forced to drift radially inward.

While these fast electron models may explain the direction of the observed rotation, whether they can account for the velocity profile evolution time scale and magnitude of E_r remains an open question. The time scale for the changes in l_i and V_{Tor} is of order of the current relaxation time (Figs.1-3). The time development of the local quantity $V_{Tor}(0)$ is found to lag behind that of the global quantity l_i, as shown in Fig.13, which is a discharge trajectory in the Δl_i - $\Delta V(0)$ plane. The points are shown for every 20 ms.

The profile (velocity, density and temperature) shapes and evolution time scales of LHCD discharges have many similarities to ICRF (and Ohmic) ITB plasmas in C-Mod. In particular, the counter-current increment in the rotation and the density profile peaking look very similar in both cases, as demonstrated in Fig.14. In the ICRF case (which entered H-mode at 0.71 s) the ITB began to develop at 0.85 s, after the plasma was in H-mode. Following this time there was an increase in the density peaking factor and a counter-current trend in the core rotation velocity. Very similar behavior is seen in the LHCD case. For LHCD however, the changes in the density and temperature

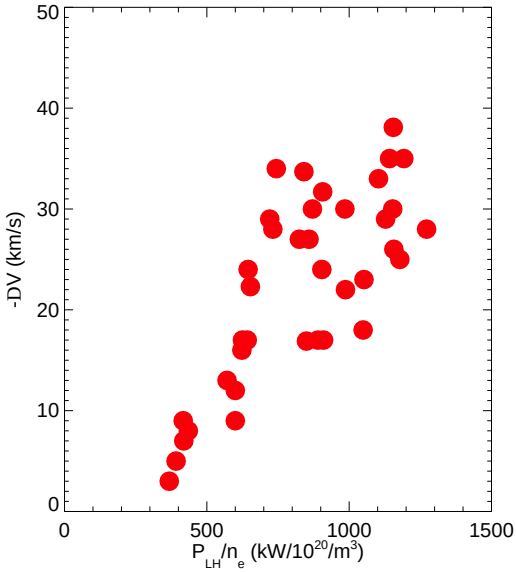

Figure 10: The change in the central rotation velocity as a function of LHCD power divided by the electron density.

profile shapes may simply be due to the inward shift of the sawtooth inversion radius (Fig.6) and not due to ITB formation. Shown in Fig.15 are the pressure and pressure gradient profiles before and during LHCD for the discharge of Figs.1 and 6. As can be seen, there is only an inward shift of the maximum pressure gradient location and only a very small increase in the gradient magnitude. TRANSP [40] simulations indicate that there is at most a 20% reduction in the core thermal conductivity after application of LHCD. These two points would suggest that the peaking of the density and temperature profiles during LHCD is not due to ITB formation, or if it is an ITB, it is a very weak one.

In summary, substantial counter-current rotation has been observed in LHCD discharges. The magnitude of the rotation is core localized and increases with LHCD power, decreases with electron density and decreases with the $n_{||}$ of the launched waves. The negative core radial electric filed is consistent with an inward shift of fast electron orbits. The rotation evolves on a time scale similar to the current relaxation time but slow compared to the momentum confinement time. The rotation is well correlated with changes in the internal inductance, and peaking of the core electron density, as well as ion and electron temperatures.

Similar effects have been observed with LHCD applied to ICRF heated H-mode target plasmas. Shown in Fig.16 are rotation velocity profiles at three different times during the discharge of Fig.4. The green $\times$s are from the Ohmic L-mode target plasma (0.6-0.7 s) and indicate a mainly flat counter-current rotation profile. The purple aster-

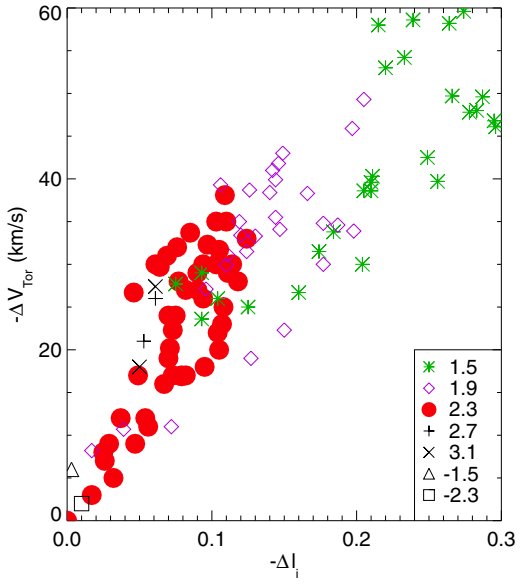

Figure 11: The change in the central rotation velocity as a function of the change in the internal inductance with LHCD. The points are sorted by $n_{||}$.

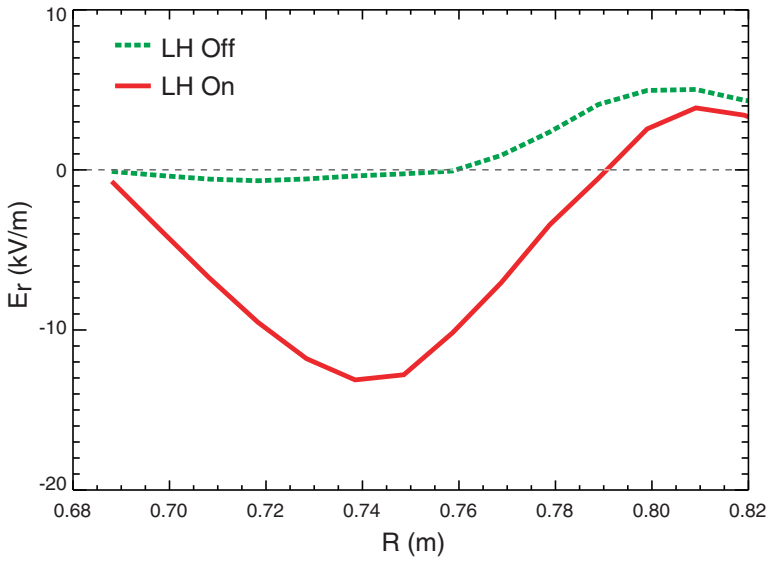

Figure 12: The radial electric field before (green dashed) and during (red solid) LHCD.

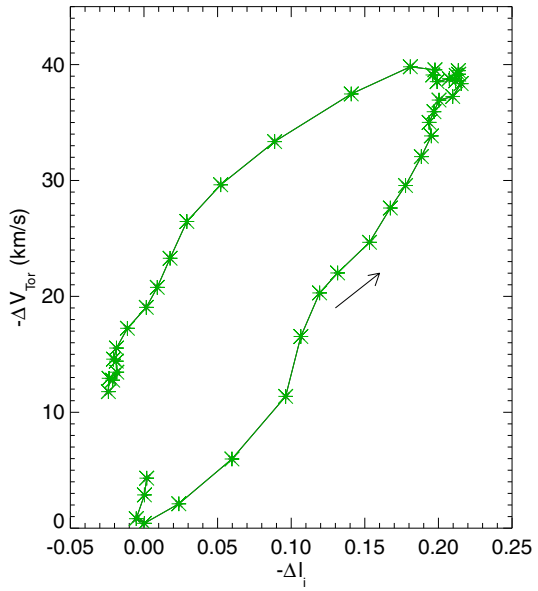

Figure 13: A LHCD plasma trajectory in the $-\Delta l_i$ - $-\Delta$V(0) plane. The points are shown for every 20 ms.

isks are from the ICRF H-mode phase (0.9-1.1 s), illustrating a relatively flat co-current rotation profile. The red points depict a hollow rotation profile during the LHCD portion (1.3-1.4 s) and demonstrate the prospect of velocity profile shape control without neutral beam injection. This latter ability may be important in future devices.

VI. Acknowledgements

The authors thank N. Fisch for enlightening discussions, J. Terry for D_α measurements and the Alcator C-Mod operations, LHCD and ICRF groups for expert running of the tokamak. Work supported at MIT by DoE Contract No. DE-FC02-99ER54512.

References

[1] N.J.Fisch, Rev. Mod. Phys. **59** (1987) 175.

[2] M.Porkolab et al., Phys. Rev. Lett. **53** (1984) 450.

[3] F.X.Soldner and JET Team, Plasma Phys. Contr. Fusion **39** (1997) B353.

[4] S.Ide et al., Nucl. Fusion **40** (2000) 445.

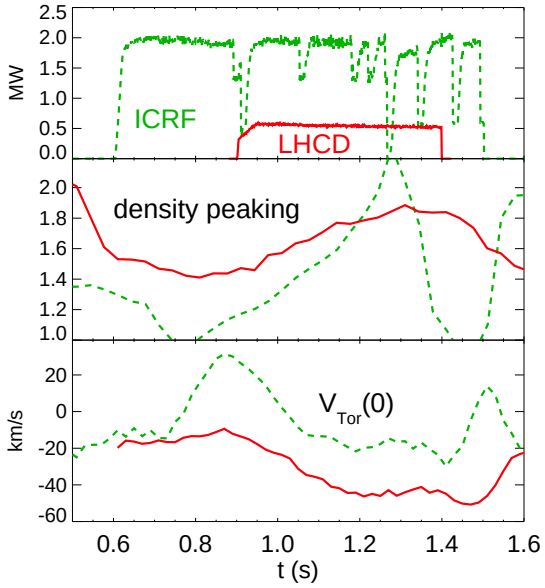

Figure 14: Auxiliary power (top), density peaking factor (middle) and central rotation velocity (bottom) for an ICRF ITB discharge (green dashed) and LHCD plasma (solid red).

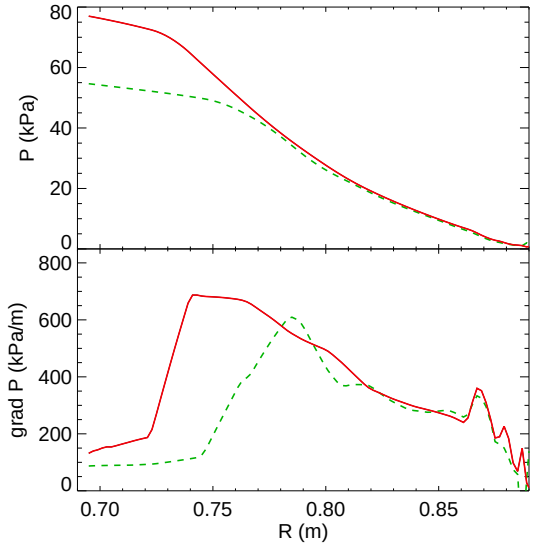

Figure 15: Pressure (top) and pressure gradient (bottom) profiles before (green dashed) and during (solid red) LHCD.

[5] P.T.Bonoli et al., Fusion Sci. Technol. **51** (2007) 401.

[6] O.Sauter et al., Phys. Plasmas **6** (1999) 2834.

[7] R.C.Wolf, Plasma Phys. Contr. Fusion **45** (2003) R1.

[8] J.W.Connor et al., Nucl. Fusion **44** (2004) R1.

[9] J.E.Rice et al., Nucl. Fusion **41** (2001) 277.

[10] C.L.Fiore et al., Phys. Plasmas **8** (2001) 2023.

[11] J.E.Rice et al., Nucl. Fusion **42** (2002) 510.

[12] S.J.Wukitch et al., Phys. Plasmas **9** (2002) 2149.

[13] J.E.Rice et al., Nucl. Fusion **43** (2003) 781.

[14] C.L.Fiore et al., Fusion Sci. Technol. **51** (2007) 303.

[15] X.Litaudon et al., Plasma Phys. Contr. Fusion **38** (1996) 1603.

[16] Z.A.Pietrzyk et al., Phys. Rev. Lett. **86** (2001) 1530.

[17] V.Pericoli Rindolfini al., Nucl. Fusion **43** (2003) 469.

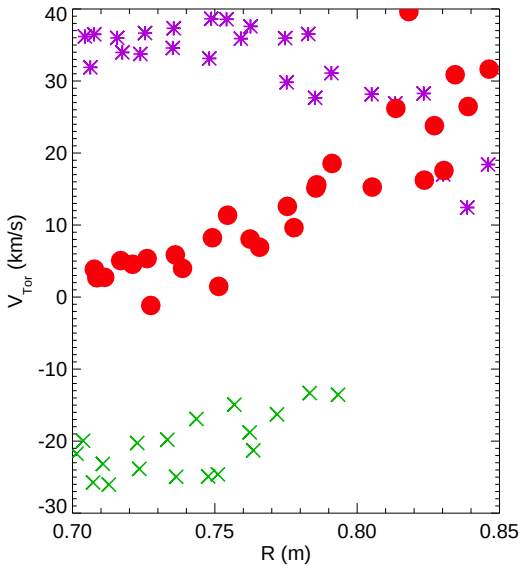

Figure 16: Rotation velocity profiles at three different times during the discharge of Fig.4. Green $\times$s Ohmic L-mode; purple asterisks ICRF H-mode; red dots ICRF H-mode with LHCD.

[18] E.J.Strait et al., Phys. Rev. Lett. **74** (1994) 2483.

[19] L.-J.Zheng et al., Phys. Rev. Lett **95** (2005) 255003.

[20] J.E.Rice et al., Nucl. Fusion **47** (2007) 1618.

[21] J.E.Rice et al., Fusion Sci. Technol. **51** (2007) 288.

[22] E.S.Marmar et al., Fusion Sci. Technol. **51** (2007) 261.

[23] A.Ince-Cushman et al., "Spatially Resolved High Resolution X-ray Spectroscopy for Magnetically Confined Fusion Plasmas", accepted for publication in Rev. Sci. Instrum. (2008).

[24] N.P.Basse et al., Fusion Sci. Technol. **51** (2007) 476.

[25] L.L.Lao et al., Nucl. Fusion **25** (1985) 1611.

[26] A.Ince-Cushman et al., "Observations of Self Generated Flows in Tokamak Plasmas with Lower Hybrid Driven Current", submitted to Phys. Rev. Lett. (2008).

[27] M.Greenwald et al., Fusion Sci. Technol. **51** (2007) 266.

[28] W.D.Lee et al., Phys. Rev. Lett. **91** (2003) 205003.

[29] J.E.Rice et al., Nucl. Fusion **44** (2004) 379.

[30] J.E.Rice et al., Nucl. Fusion **37** (1997) 421.

[31] J.E.Rice et al., Nucl. Fusion **45** (2005) 251.

[32] J.E.Rice et al., Nucl. Fusion **38** (1998) 75.

[33] J.E.Rice et al., Nucl. Fusion **39** (1999) 1175.

[34] H.Zohm et al., Plasma Phys. Contr. Fusion **33** (1991) 1423.

[35] J.A.Snipes et al., Nucl. Fusion **28** (1988) 1085.

[36] R.J.Buttery et al., Nucl. Fusion **39** (1999) 1827.

[37] A.Scarabosio et al., Plasma Phys. Contr. Fusion **48** (2006) 663.

[38] B.P.Duval et al., Plasma Phys. Contr. Fusion **49** (2007) B195.

[39] N.J.Fisch and C.F.F.Karney, Phys. Fluids **24** (1981) 27.

[40] R. J. Hawryluk, in *Proceedings of the Course in Physics Close to Thermonuclear Conditions, Varenna, 1979* (Commission of the European Communities, Brussels, 1980), Vol. I, p. 19.